RESEARCH ARTICLE | DECEMBER 04 2023

Improvement of thermoelectric performance of flexible compound $Ag_2S_{0.55}Se_{0.45}$ by means of partial V-substitution for Ag

Kosuke Sato ; Saurabh Singh ; Itsuki Yamazaki; Keisuke Hirata ; Artoni Kevin R. Ang ; Masaharu Matsunami ; Tsunehiro Takeuchi

AIP Advances 13, 125206 (2023)
https://doi.org/10.1063/5.0171888
CHORUS

Improvement of thermoelectric performance of flexible compound $Ag_2S_{0.55}Se_{0.45}$ by means of partial V-substitution for Ag

Cite as: AIP Advances 13, 125206 (2023); doi: 10.1063/5.0171888
Submitted: 11 August 2023 • Accepted: 10 November 2023 •
Published Online: 4 December 2023

Kosuke Sato,[1,a] Saurabh Singh,[1,2,a),b)] Itsuki Yamazaki,[1] Keisuke Hirata,[1] Artoni Kevin R. Ang,[1,3] Masaharu Matsunami,[1,2,3] and Tsunehiro Takeuchi[1,2,3]

AFFILIATIONS

[1] Toyota Technological Institute, Nagoya, Aichi 468-8511, Japan
[2] CREST, Japan Science and Technology Agency, Chiyoda-ku, Tokyo 102-0076, Japan
[3] MIRAI, Japan Science and Technology Agency, Chiyoda-ku, Tokyo 102-0076, Japan

[a)] **Authors to whom correspondence should be addressed:** sd21503@toyota-ti.ac.jp and saurabhsingh950@gmail.com
[b)] **Present address:** Institute of Science and Technology Austria (ISTA), Klosterneuburg 3400, Austria.

ABSTRACT

The effects of the partial V-substitution for Ag on the thermoelectric (TE) properties are investigated for a flexible semiconducting compound $Ag_2S_{0.55}Se_{0.45}$. Density functional theory calculations predict that such a partial V-substitution constructively modifies the electronic structure near the bottom of the conduction band to improve the TE performance. The synthesized $Ag_{1.97}V_{0.03}S_{0.55}Se_{0.45}$ is found to possess a TE dimensionless figure-of-merit (ZT) of 0.71 at 350 K with maintaining its flexible nature. This ZT value is relatively high in comparison with those reported for flexible TE materials below 360 K. The increase in the ZT value is caused by the enhanced absolute value of the Seebeck coefficient with less significant variation in electrical resistivity. The high ZT value with the flexible nature naturally allows us to employ the $Ag_{1.97}V_{0.03}S_{0.55}Se_{0.45}$ as a component of flexible TE generators.

I. INTRODUCTION

Thermoelectric generators (TEGs) have attracted considerable attention due to their ability in converting waste heat into useful electric power without any mechanical parts. The lack of mechanical parts makes TEGs free from regular maintenance and uncomfortable noises during the process of power generation.[1,2] The energy conversion efficiency, η, of TEGs is an increasing function of thermoelectric (TE) dimensionless figure of merit, $ZT = S^2T\rho^{-1}\kappa^{-1}$, in which T represents the absolute temperature, and S, ρ, and κ represent the Seebeck coefficient, electrical resistivity, and thermal conductivity of the constituent materials, respectively.[3] Higher values of ZT are obtainable with a larger Seebeck coefficient, a lower electrical resistivity, and a lower thermal conductivity.

At present, TEGs are expected to be power sources for bendable/wearable devices such as sensors for detecting gas leaks from pipelines[4] and monitoring human activities.[5] Such applications strongly require the flexible nature of TEG. However, the materials used in TEGs are usually brittle inorganic compounds, e.g., Bi–Te- and Pb–Te-based materials,[6,7] and hence lack deformability and malleability.

Two different kinds of flexible TEGs have been proposed. One of them is based on brittle inorganic compounds fabricated on a flexible organic substrate.[8,9] Although high ZT values are obtainable with such TE materials, the flexibility of this TEG is restricted by their brittleness. The other flexible TEG design is based on flexible organic TE materials.[10–13] In this case, all the components of this TEG are flexible, but the performance of this TEG is restricted by the low ZT values of the constituent materials, which typically possess high electrical resistivity. Thus, the development of TE materials possessing both high ZT value and flexible nature is strongly demanded.

Recently, the ductile nature was reported at room temperature (RT) for the low-temperature semiconducting phase of Ag_2S (L-Ag_2S with the Pearson symbol of $mP12$ and space group of $P2_1/c$).[14–16] This ductile nature is indeed favorable for the development of flexible TE materials. Furthermore, its very low lattice thermal conductivity of 0.5 $Wm^{-1}K^{-1}$ helps us to develop TE materials with a larger ZT.[17–19] However, its high electrical resistivity of 1.0×10^6 mΩ cm of L-Ag_2S leads to a very low ZT value of 6.3×10^{-5} at RT.[20]

To reduce the electrical resistivity, a partial Se-substitution for S in L-Ag_2S was conducted by several different groups.[20–23] The partial Se-substitution drastically increased the electron carrier concentration at RT from 1.6×10^{14} cm^{-3} in L-Ag_2S to 3.6×10^{18} cm^{-3} in $Ag_2S_{0.5}Se_{0.5}$, and the electrical resistivity of $Ag_2S_{0.5}Se_{0.5}$ was subsequently reduced to 3.3 mΩcm at RT.[20] Consequently, a relatively large ZT value of 0.26 at RT was achieved with $Ag_2S_{0.5}Se_{0.5}$ keeping the crystal structure of L-Ag_2S and the flexible nature.[20] The ZT value of $Ag_2S_{0.5}Se_{0.5}$ at RT was reported to be further improved to 0.44 by a partial substitution of Te for Se with maintaining its flexible nature.[20] However, this value is still too low to be used in various practical applications.

We employ, in this study, another approach "*a constructive modification of the electronic structure near the chemical potential by means of a partial element-substitution*" to improve the TE performance.[24,25] For this purpose, transition metals are employed as impurity elements and expected to produce impurity levels near the chemical potential of the electronic structure, leading to an improvement of the TE performance.[26–29] This approach is explained in the supplementary material (Note 1).

$Ag_2S_{1-x}Se_x$ with $x \sim 0.5$ was reported to be an n-type semiconductor with a low resistivity of ~3.3 mΩ cm at RT,[20,21] indicating that the chemical potential is near the bottom of the conduction band (CB). We expect that a modification of the bottom of CB by means of a partial element substitution would strongly affect the TE properties, resulting in an improvement of the TE performance.

In this study, we investigate the effect of the partial V-substitution for Ag on the TE properties of $Ag_2S_{1-x}Se_x$ with $x \sim 0.5$ by density functional theory (DFT) calculations and experiments. We discuss the V-substitution effects on the TE properties in terms of not only the electronic structure but also the carrier concentration.[1]

II. METHODS

A. Experimental procedure

According to the reported phase diagram,[30] the crystal structure of Ag_2S is observed in the composition range of $x < 0.6$ for $Ag_2S_{1-x}Se_x$, preserving the ductile nature of the material. However, our preliminary experiment revealed that the Ag_2Se is often precipitated in the composition range of $0.5 < x < 0.6$ for $Ag_2S_{1-x}Se_x$ due to the evaporation of S during the synthesis. To exclude such precipitation, we have chosen the slightly S-rich nominal composition: $Ag_2S_{0.55}Se_{0.45}$.

Polycrystalline $Ag_{2-x}V_xS_{0.55}Se_{0.45}$ samples with x = 0, 0.015, 0.03, and 0.06 were prepared by means of the conventional melting method. Pure Ag (purity 3N, Kojundo Chemical Laboratory), V (3N, Kojundo Chemical Laboratory), S (4N, Kojundo Chemical Laboratory), and Se (4N, Kojundo Chemical Laboratory) powders were mixed well in stoichiometric ratios using a set of agate mortar and pestle. The homogenized powder was sealed into a quartz ampoule in which the internal pressure was less than 1×10^{-2} Pa and placed in a muffle furnace. The ampoule was heated up to 1273 K in time of 8 h and maintained at 1273 K for 5 h. The heated ampoule was cooled down to 573 K in a time of 8 h and naturally cooled to RT in the furnace. Since the sample becomes brittle at low temperatures,[18,21] the obtained ingot was crushed into fine powder at the liquid nitrogen temperature using a set of alumina mortar and pestle. The obtained fine powder was densified into a pellet using the pulse current sintering method under the uniaxial pressure of 50 MPa at 673 K for 15 min. In such a process, a large electrical current that directly passes through the sample would form an inhomogeneous distribution of Ag due to the superionic nature of Ag observed in the high-temperature phase of Ag_2S (H–Ag_2S with the Pearson symbol of $cI6$ and space symmetry of $Im\bar{3}m$).[31] To prevent such an unfavorable Ag-ion conduction, the top and bottom sides of the sample were covered with insulating alumina. Table I gives the mass densities for the sintered pellets. Accordingly, all the densities of the pellets were confirmed to be at least 97% of the theoretical density.[21]

TABLE I. Mass densities of $Ag_{2-x}V_xS_{0.55}Se_{0.45}$ and the reference value of $Ag_2S_{0.5}Se_{0.5}$.[21]

x of $Ag_{2-x}V_xS_{0.55}Se_{0.45}$	Mass density (gcm^{-3})
$x = 0$	7.513
0.015	7.544
0.03	7.537
0.06	7.525
$Ag_2S_{0.5}Se_{0.5}$[21]	7.729

Phases involved in the samples at RT were identified using x-ray diffraction (XRD) measurements with conventional Cu–Kα radiation (λ = 1.54 Å) equipped in the Bruker D8 Advance and synchrotron radiation with λ = 0.62 Å at beamline BL5S2 of Aichi Synchrotron Radiation Facility, Nagoya, Japan. For the latter measurement, the sample was set into a borosilicate capillary with an inner diameter of 0.5 mm and the exposure time for each measurement was 12 min for a better signal-to-noise ratio. The Rietveld analysis[32] was conducted using RIETAN-FP[33] software to examine the effect of the partial V-substitution on the lattice constants. The quality of the Rietveld refinements was estimated by calculating R_{wp} and R_B factors, which are defined by the following equations:

$$R_{wp} = \left[\frac{\sum_i w_i (y_i - f_i)^2}{\sum_i w_i y_i^2} \right]^{\frac{1}{2}}, \quad (1)$$

$$R_B = \left[\frac{\sum_K \left| I_{obs}^K - I_{cal}^K \right|}{\sum_K I_{cal}^K} \right]^{\frac{1}{2}}, \quad (2)$$

where y_i, w_i, and f_i are the measured diffraction intensity, the weight of the observed points, and the fitting function, respectively. The I_{obs}^K and I_{cal}^K are the observed and calculated integrated intensities for the reflection $\boldsymbol{K}$, respectively.

A scanning electron microscope (SEM, Hitachi SU-6600) equipped with energy-dispersive x-ray spectroscopy (EDX, JEOL

JED-2140 GS) was used to analyze the grain structure and elemental distribution in the sample. The acceleration voltage for the SEM measurement was 20 keV. The phase transition temperature was investigated using differential scanning calorimetry (DSC, RIGAKU ThermoPlus EVO2 ESC8231).

The electrical resistivity was measured with the conventional four-probe method with a DC electrical current. The Seebeck coefficient was determined from the slope of $\Delta V - \Delta T$ plots using the steady state method with temperature differences ranging in $\Delta T = 0$–5 K. For this measurement, a K-type thermocouple was used. The typical examples of the $\Delta V - \Delta T$ plots are shown in Fig. S1. Both electrical resistivity and Seebeck coefficient were measured using homemade setups.[18,34] The uncertainties of these measurements were estimated to be within ~5%.[21,35]

The thermal conductivity, κ, was deduced from $\kappa = DC_pd$, in which D, C_p, and d represent the thermal diffusivity, specific heat, and mass density, respectively. The D and C_p were measured by the laser flash method (Netzsch LFA457)[36] while d was determined by the conventional Archimedes method (Mettler Toledo XS205 Dual Range). The uncertainty of κ was estimated to be ~7%.[21] The electronic thermal conductivity κ_{el} was calculated by the Wiedemann–Franz law,

$$\kappa_{el} = L\rho^{-1}T. \tag{3}$$

The L is the Lorentz number and defined by the following formula:[37]

$$L = \left\{1.5 + \exp\left(-\frac{|S|}{116}\right)\right\} \times 10^{-8}\left[\ \mathrm{V^2\ K^{-2}}\right]. \tag{4}$$

The lattice thermal conductivity κ_{lat} is defined by

$$\kappa_{lat} = \kappa - \kappa_{el}. \tag{5}$$

The carrier concentrations n_{car} of $Ag_2S_{0.55}Se_{0.45}$ and $Ag_{1.97}V_{0.03}S_{0.55}Se_{0.45}$ were calculated by the magnetic field-dependent Hall resistivity $\rho_{Hall}(H)$ up to $\mu_0 H = \pm 1T$ (μ_0 is the magnetic permeability in a vacuum). The $\rho_{Hall}(H)$ was measured using the conventional four-probe method with Quantum Design physical property measurement system (QD-PPMS, USA). The Hall resistivity data $\rho^{ave}_{Hall}(H)$ to calculate n_{car} was determined by

$$\rho^{ave}_{Hall}(H) = \frac{\{\rho_{Hall}(+H) - \rho_{Hall}(-H)\}}{2}. \tag{6}$$

B. DFT calculations

The chemical disorder in $Ag_2S_{0.55}Se_{0.45}$ prevents us from easily calculating electronic structure. An approximated composition of $Ag_2S_{0.5}Se_{0.5}$, with which an ordered supercell can be constructed, was employed for the DFT calculations. This composition approximation is validated in the supplementary material (Note 2). The structural model of $Ag_2S_{0.5}Se_{0.5}$ was constructed using the cell of L-Ag_2S in which eight Ag atoms and four S atoms exist. Two Se atoms were substituted for two S, as shown in Fig. 1(a).

A crystal structure model of the partially V-substituted $Ag_2S_{0.5}Se_{0.5}$ was prepared using a 2 × 2 × 1 supercell of $Ag_2S_{0.5}Se_{0.5}$, in which one of the Ag atoms was substituted by V, as shown in Fig. 1(b). The composition for the partially V-substituted $Ag_2S_{0.5}Se_{0.5}$ model was $Ag_{1.94}V_{0.06}S_{0.5}Se_{0.5}$.

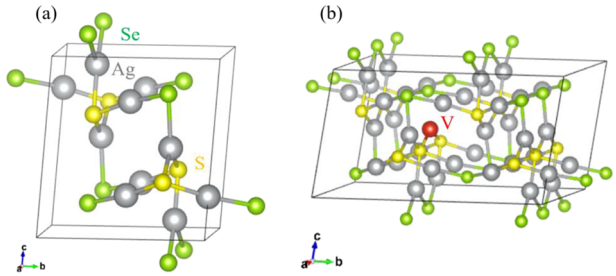

FIG. 1. Calculation models for (a) non-substituted and (b) partially V-substituted $Ag_2S_{0.5}Se_{0.5}$.

All the DFT calculations were conducted using the Vienna *ab initio* software package (VASP).[38,39] The projector augmented wave (PAW) potential[40] was used to treat interactions between the valence and core electrons. Here, we did not employ the standard Perdew–Burke–Ernzerhof functional under the generalized gradient approximation (GGA-PBE),[41] but employed the SCAN+rVV10[42] functional, which is known as a kind of meta-GGA functionals. Nam *et al.*[43] reported that although the GGA-PBE functional well reproduces the experimental bandgap of L-Ag_2S (1.1 eV), it overestimates the lattice constant of b in L-Ag_2S by 0.1 nm. They also claimed that the SCAN+rVV10 functional reproduces well both the experimental bandgap and lattice constants for L-Ag_2S. We employed, therefore, the SCAN+rVV10 functional in our DFT calculations.

Spin-unpolarized and spin-polarized calculations were performed on the non-substituted and partially V-substituted models, respectively. The energy cutoff for constructing the plane wave basis set was 400 eV. The k-mesh for the non-substituted model was 7 × 3 × 3 and 12 × 6 × 6 employed in the crystal structure optimization and density of states (DOS) calculation, respectively, while the k-mesh for the partially V-substituted model was 4 × 2 × 2 and 8 × 4 × 4 employed in the crystal structure optimization and DOS calculation, respectively. The force threshold to end the crystal structure optimization was 0.02 eV Å^{-1}.

III. RESULTS AND DISCUSSION

A. Electronic structure prediction from DFT calculations

The lattice constants of $Ag_2S_{0.5}Se_{0.5}$ were optimized by the DFT calculation. In Table II, the lattice constants are compared with the experimental data.[21] It reveals that the optimized lattice constants match the experimental ones with errors of less than 2%. Hence, we consider that the lattice constants used for the DFT calculation are reasonable.

The energy–momentum (ε–$\boldsymbol{k}$) dispersion and DOS for the non-substituted $Ag_2S_{0.5}Se_{0.5}$ are shown in Figs. 2(a) and 2(b), respectively. A direct bandgap of 0.69 eV is observable at Γ point. This value is reasonable because it is located between the experimental gaps of Ag_2S (1.1 eV)[14] and Ag_2Se (~0.1 eV).[19,44] The bandgap reduction

TABLE II. Lattice constants of $Ag_2S_{0.5}Se_{0.5}$ from the DFT calculation and experiment.[21]

	a (Å)	b (Å)	c (Å)	β (deg.)
DFT calculation	4.291	6.826	9.699	124.6
Experiment[21]	4.252	6.946	9.728	125.7

from Ag_2S to $Ag_2S_{0.5}Se_{0.5}$ is also supported by hard x-ray photoemission spectroscopy.[44] The valence band consists mainly of Ag 4*d* orbital, with minor contributions from S 3*p*, Se 4*p*, and Ag 5*s* orbitals while the CB consists of Ag 5*s*, Ag 4*d*, S 3*s*, S 3*p*, Se 4*s*, and Se 4*p* orbitals with similar intensities in DOS. The contributions of Ag 5*s* and Ag 4*d* orbitals to the CB suggest that the partial V-substitution for Ag modifies the bottom of CB.

The ε–$\boldsymbol{k}$ dispersion and DOS for the partially V-substituted $Ag_2S_{0.5}Se_{0.5}$ are illustrated in Figs. 2(c) and 2(d), respectively. According to both results, the electronic structures for the up and down spins are different from each other. The DOS for the electrons with the down spin shows no states inside the bandgap while the DOS for the electrons with the up spin shows V 3*d* states at the edge of the valence band ($\varepsilon = \varepsilon_{VBM}$), inside the bandgap ($\varepsilon = \varepsilon_{VBM} + 0.2$ eV), and near the bottom of CB ($\varepsilon = \varepsilon_{VBM} + 0.6$ eV). The chemical potential μ is expected to be near the bottom of CB according to the low electrical resistivity of $Ag_2S_{0.5}Se_{0.5}$ at RT (~3.3 mΩ cm).[20] In this case, the chemical potential can be located near the V 3*d* level, leading to the modification of the TE properties.

In the subsequent experiments, we examine if such a V 3*d* level is produced by the V-substitution and improves the *ZT* value. The carrier concentration effect on the TE properties is also discussed.

B. Structural and chemical analyses

The synchrotron powder-XRD patterns for the prepared samples with the composition of $Ag_{2-x}V_xS_{0.55}Se_{0.45}$ (x = 0, 0.015, 0.03, and 0.06) are illustrated in Fig. 3(a). The main phase for all the patterns is identified as those from the L-Ag_2S type crystal structure.[18] No peaks from secondary phases are observed in the samples with $x \leq 0.03$, but those from V (Pearson symbol of *cI*2 and space group of $Im\bar{3}m$),[45] VS (Pearson symbol of *hP*4 and space group of $P6_3/mmc$),[46] and VS_4 (Pearson symbol of *mP*40 and space group of $C2/c$)[47] are observed for the sample with x = 0.06. The solubility limit, therefore, is estimated to be less than 2 at. %, which corresponds to x = 0.06.

The lattice constants obtained by the Rietveld analysis are illustrated in Figs. 3(b)–3(d). The partial V-substitution has less significant effects on the lattice constants. The very small effects can be attributed to the low solubility limit of V in the Ag sites (less than 2 at. %). Note that the measured powder XRD data, simulated patterns, the difference between simulated and measured patterns, peak positions, R_{wp}-factor, and R_B-factor are shown in Fig. S2.

The DSC results for $Ag_{2-x}V_xS_{0.55}Se_{0.45}$ (x = 0, 0.015, and 0.03) are shown in Fig. 3(e). The $Ag_2S_{0.55}Se_{0.45}$ possesses an endothermic peak at 365 K, which is close to the reported transition temperature of 355 K for $Ag_2S_{0.5}Se_{0.5}$.[20] Within the solubility limit (less than 2 at. %), the partial V-substitution for Ag leads to a monotonic increase in the phase transition temperature. Such behavior suggests

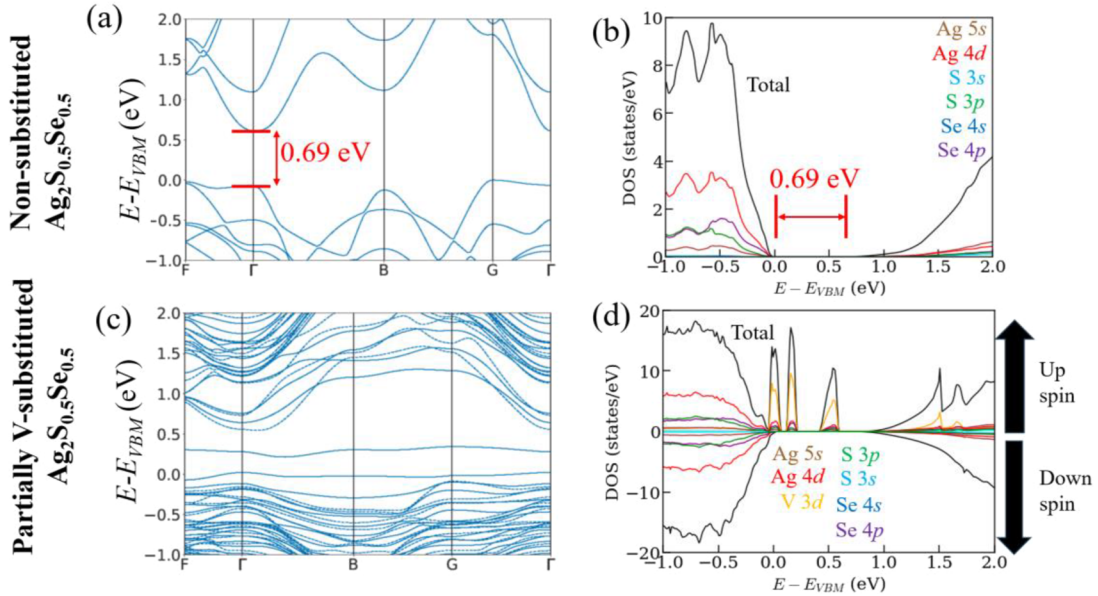

FIG. 2. (a) Energy–momentum dispersion and (b) total (black) and projected DOS (the other colors) for non-substituted $Ag_2S_{0.5}Se_{0.5}$. (c) Energy–momentum dispersion for the partially V-substituted $Ag_2S_{0.5}Se_{0.5}$. The solid and dashed lines correspond to the dispersions of electrons with up and down spins, respectively. (d) Total (black) and projected (the other colors) DOS for the partially V-substituted $Ag_2S_{0.5}Se_{0.5}$. The upper and lower lines correspond to the DOS for electrons with up and down spins, respectively.

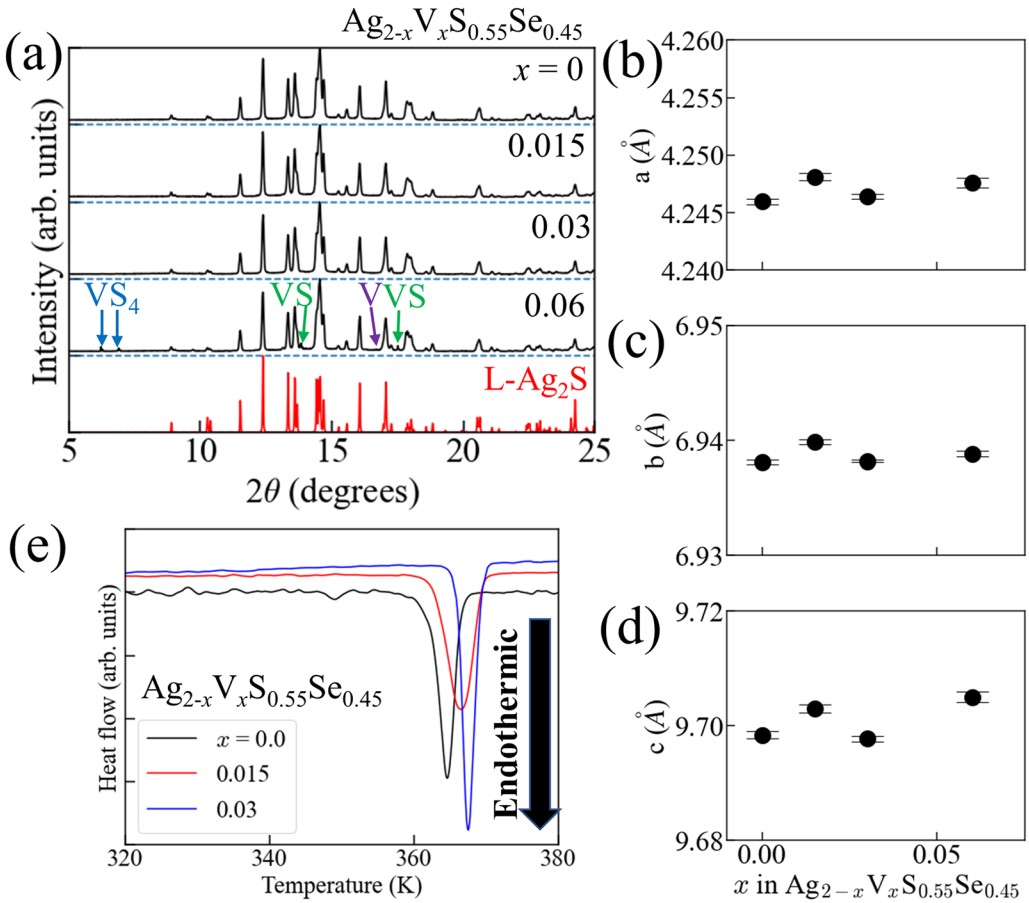

FIG. 3. (a) Synchrotron powder-XRD patterns measured for $Ag_{2-x}V_xS_{0.55}Se_{0.45}$ with x = 0, 0.015, 0.03, and 0.06. Simulated XRD patterns of L-Ag_2S[18] and peak positions from V,[45] VS,[46] and VS_4[47] are also shown. (b)–(d) Lattice constants of (b) *a*, (c) *b*, and (d) *c* obtained by the Rietveld analysis. (e) DSC results for $Ag_{2-x}V_xS_{0.55}Se_{0.45}$ with x = 0, 0.015, and 0.03.

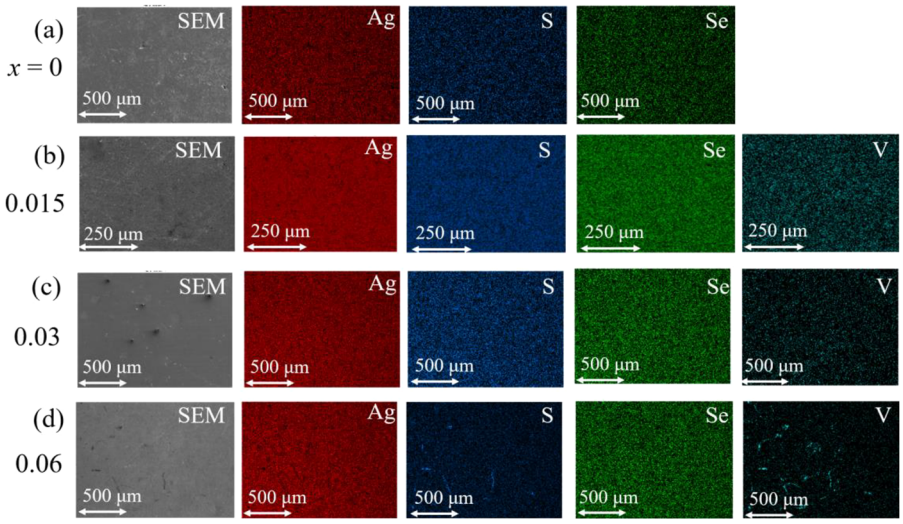

FIG. 4. SEM images and EDX mappings for $Ag_{2-x}V_xS_{0.55}Se_{0.45}$ with x = (a) 0, (b) 0.015, (c) 0.03, and (d) 0.06.

that V is properly substituted for Ag and affects the free energies of $Ag_2S_{0.55}Se_{0.45}$.

The SEM images together with the EDX elemental mappings are shown in Fig. 4. We find no cracks and voids in all the samples. In addition, uniform distributions of the elements are observed with $x = 0.0$, 0.015, and 0.03 while the precipitations of V and its sulfides are observed with $x = 0.06$. These results are consistent with the solubility limit of 2 at. % estimated by the XRD measurement [Fig. 3(a)]. We already confirmed the consistency of the Cu–Kα XRD patterns for the powders and pellets of $Ag_{2-x}V_xS_{0.55}Se_{0.45}$ (x = 0, 0.015, 0.03 and 0.06): a typical example is shown in Fig. S3. Therefore, these results indicate that the characteristics of the pellets and powder are consistent.

C. TE properties and performance

The temperature and composition dependences of the electrical resistivity are shown in Figs. 5(a) and 5(b), respectively. The electrical resistivity of the sample with $x = 0$ decreases with increasing temperature. This behavior is related to the electron–hole excitation in typical semiconductors. We also note that the V-substitution provides little effect on the trend of the temperature dependence of electrical resistivity. The electrical resistivity of $Ag_2S_{0.55}Se_{0.45}$ is 6.38 mΩ cm at 316 K, which is comparable with the reported value of ~3 mΩ cm for $Ag_2S_{0.5}Se_{0.5}$ at 316 K.[20] Such a low electrical resistivity suggests that the chemical potential is located near the bottom of CB. The V-substitution with $x = 0.015$ and 0.03 makes the electrical resistivity only slightly higher than the value with $x = 0$. More

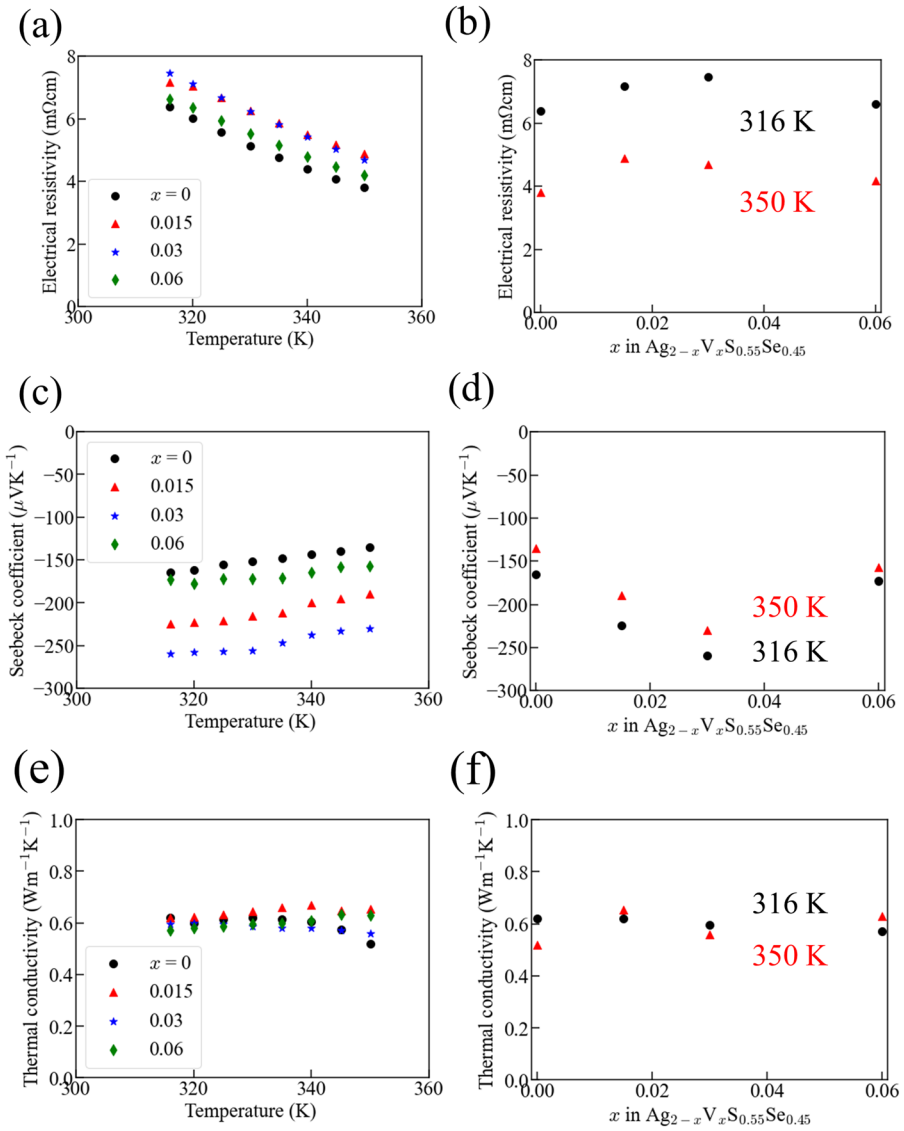

FIG. 5. (a) Temperature and (b) composition dependences of the electrical resistivity, (c) temperature and (d) composition dependences of the Seebeck coefficient, and (e) temperature and (f) composition dependences of the thermal conductivity for $Ag_{2-x}V_xS_{0.55}Se_{0.45}$ with x = 0, 0.015, 0.03, and 0.06.

V-substitutions (x = 0.06) lead to a reduction in the magnitude of the electrical resistivity from those with x = 0.015 and 0.03. This reduction can be attributed to the precipitations of V and its sulfides observed in Figs. 3(a) and 4(d).

The temperature and composition dependences of the Seebeck coefficient are shown in Figs. 5(c) and 5(d), respectively. The absolute value of the Seebeck coefficient for all the cases decreases with increasing temperature. This trend is consistent with the temperature dependence of electrical resistivity [Fig. 5(a)]. Notably, the absolute value of the Seebeck coefficient becomes significantly enhanced by V-substitution with x = 0.015 and 0.03. The $Ag_{2-x}V_xS_{0.55}Se_{0.45}$ with x = 0.06 possesses the absolute value of the Seebeck coefficient smaller than that with x = 0.015 and 0.03. This reduction can be attributed to the precipitations of V and its sulfides and is consistent with the electrical resistivity shown in Fig. 5(b).

The V-substitution with x = 0.03 makes the absolute value of the Seebeck coefficient ~1.6 times larger from −165 to −259 μV K^{-1} at 316 K, but makes the electrical resistivity only ~1.2 times larger from 6.38 to 7.46 mΩ cm at 316 K. Consequently, the power factor ($PF = S^2\rho^{-1}$) at 316 K is ~2.1 times larger by the V-substitution with x = 0.03. To clarify the carrier concentration effect on this larger power factor, the carrier concentrations were estimated by the measurements of the magnetic field-dependent Hall resistivity. No significant differences in the carrier concentrations of $Ag_2S_{0.55}Se_{0.45}$ (7.7×10^{18} cm^{-3}) and $Ag_{1.97}V_{0.03}S_{0.55}Se_{0.45}$ (1.1×10^{19} cm^{-3}) were observed, suggesting that the larger power factor is not attributed to the difference in the carrier concentration, but to the modification of the electronic structure near the chemical potential by the V-substitution.

The electrical resistivity for $Ag_{1.97}V_{0.03}S_{0.55}Se_{0.45}$ is also low (less than 8 mΩ cm at T < 350 K), indicating that the chemical potential is still near the bottom of CB. Following our prediction from the DFT calculations, the V 3d state is located around the bottom of CB. Considering the obtained results that the V-substitution (0.5 and 1 at. %) enlarges significantly the Seebeck coefficient but slightly the electrical resistivity, with the Boltzmann transport equation [Eqs. (S1), (S2), and (S5)], we conclude that the V 3d state is distributed at $\varepsilon = \mu + 1.6k_BT$, but not at $\varepsilon = \mu$.

The temperature and composition dependences of the thermal conductivity are illustrated in Figs. 5(e) and 5(f), respectively. For x = 0, the thermal conductivity ranges from 0.5 – 0.65 Wm^{-1} K^{-1} regardless of the temperature. This value is comparable with that reported for $Ag_2S_{0.5}Se_{0.5}$ (~0.5 Wm^{-1} K^{-1}) at RT.[21] The low thermal conductivity can be attributed to the anharmonic vibration of Ag ions.[21] The V-substitution is found to cause a less significant effect on the thermal conductivity. This result indicates that the anharmonic vibration of Ag ions and the corresponding lattice thermal conductivity are insensitive to the local V-substitution. The electronic and lattice thermal conductivities were calculated using Eqs. (3)–(5) and the results are shown in Fig. S4. The results show that the lattice thermal conductivity is around 0.5 Wm^{-1} K^{-1}. This value is consistent with the reported value for $Ag_2S_{1-x}Se_x$ system.[21] The very low lattice thermal conductivity observed at 350 K for $Ag_2S_{0.55}Se_{0.45}$ can be attributed to the effect of the phase transition.[48]

Finally, the effects of V-substitution on the PF and ZT of $Ag_2S_{0.55}Se_{0.45}$ are illustrated in Figs. 6(a) and 6(b), respectively. As already discussed, the PF is improved by the V-substitution of 1 at. % (x = 0.03). At 350 K, the PF value becomes ~2.5 times larger from 0.48 mW m^{-1} K^{-2} for $Ag_2S_{0.55}Se_{0.45}$ to 1.1 mW m^{-1} K^{-2} for

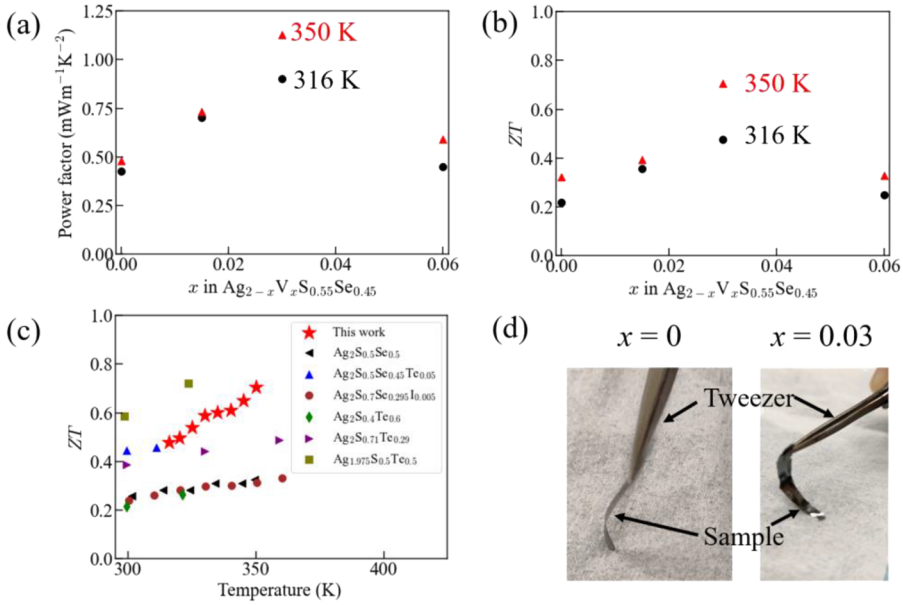

FIG. 6. Composition dependence of (a) PF and (b) ZT of $Ag_{2-x}V_xS_{0.55}Se_{0.45}$ at 316 and 355 K. (c) ZT values of $Ag_{1.97}V_{0.03}S_{0.55}Se_{0.45}$ with reported values for the flexible compounds: $Ag_2S_{0.5}Se_{0.5}$,[20] $Ag_2S_{0.5}Se_{0.45}Te_{0.05}$,[20] $Ag_2S_{0.7}Se_{0.295}I_{0.005}$,[23] $Ag_2S_{0.4}Te_{0.6}$,[49] $Ag_2S_{0.71}Te_{0.29}$,[50] and $Ag_{1.975}S_{0.5}Te_{0.5}$.[51] (d) Bent thin pieces made of the bulk $Ag_{2-x}V_xS_{0.55}Se_{0.45}$ with x = 0 and 0.03.

$Ag_{1.97}V_{0.03}S_{0.55}Se_{0.45}$. The ZT value at 350 K also increases ~2.2 times larger from 0.32 for $Ag_2S_{0.55}Se_{0.45}$ to 0.71 for $Ag_{1.97}V_{0.03}S_{0.55}Se_{0.45}$. Therefore, our scenario that the V-substitution constructively modifies the bottom of CB and improves the TE performance of $Ag_2S_{0.55}Se_{0.45}$ is validated.

In Fig. 6(c), the temperature dependence of the ZT values for $Ag_{1.97}V_{0.03}S_{0.55}Se_{0.45}$ is compared to those reported from other flexible inorganic TE materials: $Ag_2S_{0.5}Se_{0.5}$,[20] $Ag_2S_{0.5}Se_{0.45}Te_{0.05}$,[20] $Ag_2S_{0.7}Se_{0.295}I_{0.005}$,[23] $Ag_2S_{0.4}Te_{0.6}$,[49] $Ag_2S_{0.71}Te_{0.29}$,[50] and $Ag_{1.975}S_{0.5}Te_{0.5}$.[51] We find that the ZT values of $Ag_{1.97}V_{0.03}S_{0.55}Se_{0.45}$ are relatively high in comparison with the reported values at temperatures less than 360 K. It should be mentioned in addition that $Ag_{1.97}V_{0.03}S_{0.55}Se_{0.45}$ possesses the flexibility like $Ag_2S_{0.55}Se_{0.45}$ as shown in Fig. 6(d) and that the TE performance of $Ag_{1.97}V_{0.03}S_{0.55}Se_{0.45}$ remains even after hundreds of the bending cycles as explained in the supplementary material (Note 3) with Fig. S5.[52,53] Therefore, we expect that $Ag_{1.97}V_{0.03}S_{0.55}Se_{0.45}$ can be used in future flexible TEGs.

IV. CONCLUSIONS

We tried to improve the TE performance of $Ag_2S_{0.55}Se_{0.45}$ by partial element substitution for Ag. From the DFT calculations, we predicted that the partial V-substitution for Ag produced V 3d states at the bottom of the CB. Such V 3d states were expected to affect the TE properties and lead to an improvement in the TE performance. Experimentally, we revealed that 1 at. % V-substitution (x = 0.03 of $Ag_{2-x}V_xS_{0.55}Se_{0.45}$) increased the power factor by a factor of ~2.3 at 350 K. This increase was caused by the significant increase in the absolute value of the Seebeck coefficient with less significant variation in the electrical resistivity. The larger power factor was attributed not to the change of the carrier concentration but to the V 3d states at the bottom of CB. With the help of the low thermal conductivity of 0.5–0.65 Wm^{-1} K^{-1}, the ZT value of $Ag_{1.97}V_{0.03}S_{0.55}Se_{0.45}$ reached 0.71 at 350 K. The obtained ZT values were found relatively high in comparison with those reported for other flexible TE materials below 360 K. From these results, we suggest that $Ag_{1.97}V_{0.03}S_{0.55}Se_{0.45}$ can be utilized for the development of flexible TEGs suitable in the energy harvesting applications in the future.

SUPPLEMENTARY MATERIAL

See the supplementary material: the $\Delta V - \Delta T$ relationships for $Ag_2S_{0.55}Se_{0.45}$ and $Ag_{1.97}V_{0.03}S_{0.55}Se_{0.45}$ in Fig. S1; the observed synchrotron powder XRD data, simulated patterns, the difference between simulated and observed patterns, peak position, R_{wp}-factor, and R_B-factor in Fig. S2; XRD patterns for the powder and pellet of $Ag_2S_{0.55}Se_{0.45}$ in Fig. S3; electronic and lattice thermal conductivities of $Ag_{2-x}V_xS_{0.55}Se_{0.45}$ in Fig. S4; bending cycle dependence of the electrical resistivity and Seebeck coefficient in Fig. S5; window functions of W_0, W_1, and W_2 in Fig. S6; band structures and gaps of Ag_2S, $Ag_2S_{0.75}Se_{0.25}$, and $Ag_2S_{0.5}Se_{0.5}$ in Fig. S7; the method of the constructive modification of the electronic structure near the chemical potential in Supplementary Note 1; the validity of the approximation of the composition ($Ag_2S_{0.55}Se_{0.45}$ → $Ag_2S_{0.5}Se_{0.5}$) in Supplementary Note 2; and the description about bending cycle dependence of the electrical resistivity and Seebeck coefficient in Supplementary Note 3.

ACKNOWLEDGMENTS

This work received financial support partially from Japan Science and Technology Agency (JST) CREST Grant No. JPMJCR18I2, Japan. The powder-XRD experiments were conducted at BL5S2 of Aichi Synchrotron Radiation Center, Aichi Science & Technology Foundation, Aichi, Japan (Proposal No. 202301057).

AUTHOR DECLARATIONS

Conflict of Interest

The authors have no conflicts to disclose.

Author Contributions

Kosuke Sato: Conceptualization (lead); Data curation (lead); Formal analysis (lead); Investigation (lead); Validation (lead); Visualization (lead); Writing – original draft (lead); Writing – review & editing (lead). **Saurabh Singh**: Conceptualization (equal); Investigation (equal); Resources (lead); Writing – review & editing (supporting). **Itsuki Yamazaki**: Investigation (supporting); Validation (equal). **Keisuke Hirata**: Formal analysis (supporting); Investigation (supporting); Resources (equal). **Artoni Kevin R. Ang**: Investigation (supporting); Writing – review & editing (supporting). **Masaharu Matsunami**: Supervision (supporting); Writing – review & editing (supporting). **Tsunehiro Takeuchi**: Funding acquisition (lead); Project administration (lead); Resources (equal); Supervision (lead); Writing – review & editing (lead).

DATA AVAILABILITY

The data that support the findings of this study are available from the corresponding authors upon reasonable request.

REFERENCES

[1] G. J. Snyder and E. S. Toberer, Nat. Mater. **7**, 105 (2008).
[2] Q. Yan and M. G. Kanatzidis, Nat. Mater. **21**, 503 (2022).
[3] T. Takeuchi, Mater. Trans. **50**, 2359 (2009).
[4] K. Yazawa, Y. Feng, and N. Lu, Energy Convers. Manage. **244**, 114487 (2021).
[5] S. C. Mukhopadhyay, IEEE Sens. J. **15**, 1321 (2015).
[6] S. I. Kim, K. H. Lee, H. A. Mun, H. S. Kim, S. W. Hwang, J. W. Roh, D. J. Yang, W. H. Shin, X. S. Li, Y. H. Lee *et al.*, Science **348**, 109 (2015).
[7] K. Biswas, J. He, I. D. Blum, C.-I. Wu, T. P. Hogan, D. N. Seidman, V. P. Dravid, and M. G. Kanatzidis, Nature **489**, 414 (2012).
[8] Q. Jin, S. Jiang, Y. Zhao, D. Wang, J. Qiu, D.-M. Tang, J. Tan, D.-M. Sun, P.-X. Hou, X.-Q. Chen, K. Tai, N. Gao, C. Liu, H.-M. Cheng, and X. Jiang, Nat. Mater. **18**, 62 (2019).
[9] T. Sugahara, Y. Ekubaru, N. V. Nong, N. Kagami, K. Ohata, L. T. Hung, M. Okajima, S. Nambu, and K. Suganuma, Adv. Mater. Technol. **4**, 1800556 (2019).
[10] G.-H. Kim, L. Shao, K. Zhang, and K. P. Pipe, Nat. Mater. **12**, 719 (2013).
[11] Q. Yao, Q. Wang, L. Wang, and L. Chen, Energy Environ. Sci. **7**, 3801 (2014).
[12] Q. Zhang, Y. Sun, W. Xu, and D. Zhu, Macromolecules **47**, 609 (2014).

[13]S. Qu, Q. Yao, L. Wang, Z. Chen, K. Xu, H. Zeng, W. Shi, T. Zhang, C. Uher, and L. Chen, NPG Asia Mater. **8**, e292 (2016).
[14]X. Shi, H. Chen, F. Hao, R. Liu, T. Wang, P. Qiu, U. Burkhardt, Y. Grin, and L. Chen, Nat. Mater. **17**, 421 (2018).
[15]G. Li, Q. An, S. I. Morozov, B. Duan, W. A. Goddard, Q. Zhang, P. Zhai, and G. J. Snyder, Npj Comput. Mater. **4**, 44 (2018).
[16]M. Misawa, H. Hokyo, S. Fukushima, K. Shimamura, A. Koura, F. Shimojo, R. K. Kalia, A. Nakano, and P. Vashishta, Sci. Rep. **12**, 19458 (2022).
[17]K. Hirata, T. Matsunaga, S. Singh, M. Matsunami, and T. Takeuchi, J. Electron. Mater. **49**, 2895 (2020).
[18]G. Kim, D. Byeon, S. Singh, K. Hirata, S. Choi, M. Matsunami, and T. Takeuchi, J. Phys. D: Appl. Phys. **54**, 115503 (2021).
[19]K. Hirata, T. Matsunaga, S. Saurabh, M. Matsunami, and T. Takeuchi, Mater. Trans. **61**, 2402 (2020).
[20]J. Liang, T. Wang, P. Qiu, S. Yang, C. Ming, H. Chen, Q. Song, K. Zhao, T.-R. Wei, D. Ren, Y.-Y. Sun, X. Shi, J. He, and L. Chen, Energy Environ. Sci. **12**, 2983 (2019).
[21]K. Hirata, S. Singh, and T. Takeuchi, AIP Adv. **13**, 35122 (2023).
[22]S. Singh, K. Hirata, D. Byeon, T. Matsunaga, O. Muthusamy, S. Ghodke, M. Adachi, Y. Yamamoto, M. Matsunami, and T. Takeuchi, J. Electron. Mater. **49**, 2846 (2020).
[23]J. Liu, T. Xing, Z. Gao, J. Liang, L. Peng, J. Xiao, P. Qiu, X. Shi, and L. Chen, Appl. Phys. Lett. **119**, 121905 (2021).
[24]J. P. Heremans, V. Jovovic, E. S. Toberer, A. Saramat, K. Kurosaki, A. Charoenphakdee, S. Yamanaka, and G. J. Snyder, Science **321**, 554 (2008).
[25]J. P. Heremans, B. Wiendlocha, and A. M. Chamoire, Energy Environ. Sci. **5**, 5510 (2012).
[26]A. Yamamoto, H. Miyazaki, M. Inukai, Y. Nishino, and T. Takeuchi, Jpn. J. Appl. Phys. **54**, 71801 (2015).
[27]A. Yamamoto and T. Takeuchi, J. Electron. Mater. **46**, 3200 (2017).
[28]K. Delime-Codrin, M. Omprakash, S. Ghodke, R. Sobota, M. Adachi, M. Kiyama, T. Matsuura, Y. Yamamoto, M. Matsunami, and T. Takeuchi, Appl. Phys. Express **12**, 45507 (2019).
[29]O. Muthusamy, S. Singh, K. Hirata, K. Kuga, S. K. Harish, M. Shimomura, M. Adachi, Y. Yamamoto, M. Matsunami, and T. Takeuchi, ACS Appl. Electron. Mater. **3**, 5621 (2021).
[30]S. Miyatani, J. Phys. Soc. Jpn. **15**, 1586 (1960).
[31]S. I. Sadovnikov and E. Y. Gerasimov, Nanoscale Adv. **1**, 1581 (2019).
[32]D. E. Cox, J. B. Hastings, W. Thomlinson, and C. T. Prewitt, Nucl. Instrum. Methods Phys. Res. **208**, 573 (1983).
[33]F. Izumi and K. Momma, Solid State Phenom. **130**, 15 (2007).
[34]S. Singh and S. K. Pandey, IEEE Trans. Instrum. Meas. **67**, 2169 (2018).
[35]A. Kumar, A. Patel, S. Singh, A. Kandasami, and D. Kanjilal, Rev. Sci. Instrum. **90**, 104901 (2019).
[36]S. Min, J. Blumm, and A. Lindemann, Thermochim. Acta **455**, 46 (2007).
[37]H.-S. Kim, Z. M. Gibbs, Y. Tang, H. Wang, and G. J. Snyder, APL Mater. **3**, 41506 (2015).
[38]G. Kresse and J. Hafner, Phys. Rev. B **49**, 14251 (1994).
[39]G. Kresse and J. Furthmüller, Comput. Mater. Sci. **6**, 15 (1996).
[40]G. Kresse and D. Joubert, Phys. Rev. B **59**, 1758 (1999).
[41]J. P. Perdew, K. Burke, and M. Ernzerhof, Phys. Rev. Lett. **77**, 3865 (1996).
[42]H. Peng, Z.-H. Yang, J. P. Perdew, and J. Sun, Phys. Rev. X **6**, 41005 (2016).
[43]H. N. Nam, R. Yamada, H. Okumura, T. Q. Nguyen, K. Suzuki, H. Shinya, A. Masago, T. Fukushima, and K. Sato, Phys. Chem. Chem. Phys. **23**, 9773 (2021).
[44]K. Sato, K. Hirata, S. Singh, K. Kuga, F. Ogawa, M. Matsunami, and T. Takeuchi, J. Appl. Phys. **132**, 45104 (2022).
[45]M. E. Straumanis, J. Appl. Phys. **30**, 1965 (1959).
[46]P. Rahlfs, Z. Phys. Chem. **31B**, 157 (1936).
[47]R. Allmann, I. Baumann, A. Kutoglu, H. Rösch, and E. Hellner, Naturwissenschaften **51**, 263 (1964).
[48]H. Chen, Z. Yue, D. Ren, H. Zeng, T. Wei, K. Zhao, R. Yang, P. Qiu, L. Chen, and X. Shi, Adv. Mater. **31**, 1806518 (2019).
[49]S. He, Y. Li, L. Liu, Y. Jiang, J. Feng, W. Zhu, J. Zhang, Z. Dong, Y. Deng, J. Luo, W. Zhang, and G. Chen, Sci. Adv. **6**, eaaz8423 (2020).
[50]S. Yang, Z. Gao, P. Qiu, J. Liang, T.-R. Wei, T. Deng, J. Xiao, X. Shi, and L. Chen, Adv. Mater. **33**, 2007681 (2021).
[51]X. Liang and C. Chen, Acta Mater. **218**, 117231 (2021).
[52]S. Yang, P. Qiu, L. Chen, and X. Shi, Small Sci. **1**, 2100005 (2021).
[53]S. Y. Tee, D. Ponsford, C. L. Lay, X. Wang, X. Wang, D. C. J. Neo, T. Wu, W. Thitsartarn, J. C. C. Yeo, G. Guan, T.-C. Lee, and M.-Y. Han, Adv. Sci. **9**, 2204624 (2022).